ELECTRON EXCITATION OF NUCLEON RESONANCES*

By J. D. Walecka

Institute of Theoretical Physics, Stanford University**

(*Presented at the XIth Cracow School of Theoretical Physics, Zakopane, June 8–22, 1971*)

The general analysis of electron excitation of nucleon resonances is presented, and the consequences of two very simple models of the nucleon are discussed. The results are compared with SLAC data on this process.

1. General analysis

A. Introduction
B. Response surfaces with single-photon exchange
   i) Electron scattering
   ii) Photoabsorption
C. Some SLAC results in the resonance region
   i) Response surfaces
   ii) Inelastic form factors
D. Analysis of excitation of diserete states
   i) Helicity analysis and inelastic form factors
   ii) Cross section
   iii) Threshold behavior
E. Pion electroproduction
   i) Expansion in kinematic invariants
   ii) Helicity analysis
   iii) Identification of inelastic form factors

There are two reasons why electron scattering is a powerful tool for studying nuclear structure. First, the interaction is known. The electron interacts with the local electromagnetic current density in the target. Since this interaction is relatively weak, of order α, one can make measurements without greatly disturbing the structure of the target,

* Research sponsored by the Air Force Office of Scientific Research, Office of Aerospace Research, U.S. Air Force, under AFOSR Contract No F44620-68-C-0075.

** Address: Department of Physics, Institute of Theoretical Physics, Stanford University, Stanford, California 94305, USA.

in contrast to the situation in the scattering of hadrons. Second, for a fixed energy transfer, the three-momentum can be varied and the Fourier transforms of the transition charge and current densities mapped out.

The present discussion will be limited almost entirely to the situation where only the electron is detected. In this case there are three free variables, k_1 and k_2, the initial and final electron wave numbers, and θ the scattering angle, or equivalently $\kappa^2 = (k_2 - k_1)^2$, $W^2 = -(P-\kappa)^2$, the masses of the virtual photon and final state of the target, and θ. If the target

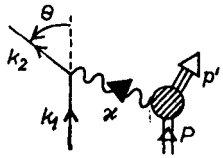

is unobserved, then in the one-photon-exchange approximation the cross-section can be calculated in the standard fashion and takes the form[1] [1]

$$\frac{d^2\sigma}{d\Omega_2 d\varepsilon_2} = \frac{\alpha^2}{4\varepsilon_1^2 \sin^4 \frac{\theta}{2}} \cdot \frac{1}{m} \cdot L_{\mu\nu} W_{\mu\nu} \tag{1.1}$$

where

$$L_{\mu\nu} = -\tfrac{1}{2} \sum_{\text{spins}} \bar{u}(k_2)\gamma_\mu u(k_1)\bar{u}(k_1)\gamma_\nu u(k_2) =$$

$$= \frac{1}{2\varepsilon_1 \varepsilon_2} [k_{1\mu}k_{2\nu} + k_{1\nu}k_{2\mu} - \delta_{\mu\nu}(k_1 \cdot k_2)] \tag{1.2}$$

and the target response is characterized by the tensor

$$W_{\mu\nu} = (2\pi)^3 \Omega \overline{\sum_i} \sum_f \delta^{(4)}(P - P' - \kappa) \langle P | \hat{J}_\nu(0) | P' \rangle \langle P' | \hat{J}_\mu(0) | P \rangle (E) = \tag{1.3}$$

$$= W_1(\kappa^2, \kappa \cdot P)\left(\delta_{\mu\nu} - \frac{\kappa_\mu \kappa_\nu}{\kappa^2}\right) + W_2(\kappa^2, \kappa \cdot P) \frac{1}{m^2}\left(P_\mu - \frac{P \cdot \kappa}{\kappa^2}\kappa_\mu\right)\left(P_\nu - \frac{P \cdot \kappa}{\kappa^2}\kappa_\nu\right) \tag{1.4}$$

where Ω is the normalization volume, E is the initial energy of the target, m is the target mass, $\overline{\sum}$ indicates an average over initial target, states, $|P\rangle$ and $|P'\rangle$ are Heisenberg state vectors of the initial and final target states and $\hat{J}_\mu(0)$ is the electromagnetic current operator for the target evaluated at $x_\mu = 0$. The form (1.4) follows from Lorentz covariance and current conservation [2], and the electromagnetic response of any target is evidently characterized by two response surfaces $W_{1,2}(\kappa^2, \kappa \cdot P)$. The electron scattering

[1] We use a metric such that $a_\mu = (\boldsymbol{a}, ia_0)$. The gamma matrices are hermitian and satisfy $\gamma_\mu\gamma_\nu + \gamma_\nu\gamma_\mu = 2\delta_{\mu\nu}$. The Dirac equation is $(i\gamma \cdot p + m_e)u(p) = 0$. We also take $\hbar = c = 1$ and $\alpha = e^2/4\pi \cong 1/137$. We use a carat to denote operators in the Hilbert space of the target.

cross-section is thus

$$\frac{d^2\sigma}{d\Omega_2 d\varepsilon_2} = \frac{\alpha^2 \cos^2 \frac{\theta}{2}}{4\varepsilon_1^2 \sin^4 \frac{\theta}{2}} \cdot \frac{1}{m} \cdot \left[W_2(\kappa^2, \kappa \cdot P) + 2W_1(\kappa^2, \kappa \cdot P) \tan^2 \frac{\theta}{2} \right]. \tag{1.5}$$

The contributions $W_{1,2}$ can be separated by keeping the variables κ^2 and $\kappa \cdot P$ fixed and making a straight-line plot against $\tan^2 \frac{\theta}{2}$ (a "Rosenbluth plot") or by working at $\theta = 180°$ where only W_1 contributes.

The same response tensor $W_{\mu\nu}$ describes the absorption of a real photon of four-momentum $k \equiv -\kappa$, and the photoabsorption cross-section again follows in a straightforward manner

$$\sigma_\gamma(\omega) = \frac{(2\pi)^2 \alpha}{m\omega} \cdot \frac{1}{2} \sum_{\text{pol}} e_\mu^{(\lambda)} W_{\mu\nu} e_\nu^{(\lambda)} =$$

$$= \frac{(2\pi)^2 \alpha}{m\omega} \cdot W_1(0, -k \cdot P) \tag{1.6}$$

where $m\omega \equiv -k \cdot P$. Thus photoabsorption measures one slice at $\kappa^2 = 0$ on the two-dimensional surfaces $W_{1,2}(\kappa^2, \kappa \cdot P)$.

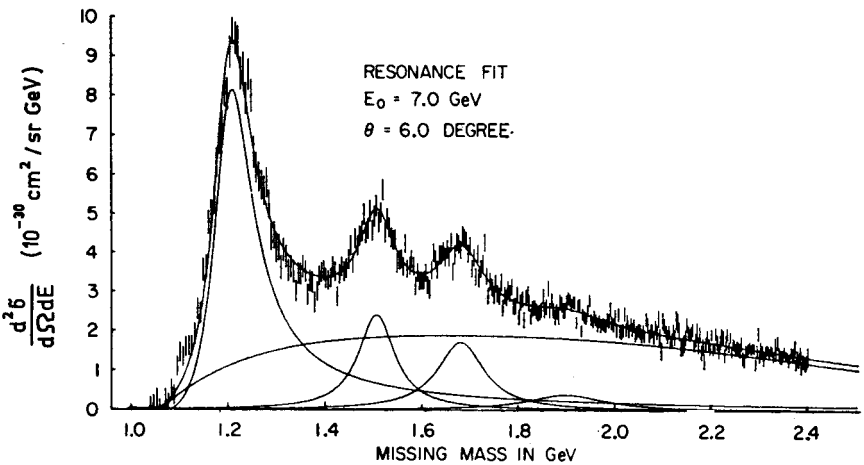

Fig. 1. The SLAC experimental inelastic spectrum at $\varepsilon_1 = 7$ GeV, $\theta = 6°$, resolved into Breit-Wigner resonances by the fitting procedure discussed in the text [3]

Figures 1 and 2 show measurements of the SLAC group of the (radiatively corrected) cross-section for inelastic electron scattering from the proton at $\theta = 6°$ and incident energies $\varepsilon_1 = 7$ and 10 GeV [3, 4]. The elastic peak is not shown on these figures. There are three distinct, and a fourth discernable, peaks seen in these experiments corresponding

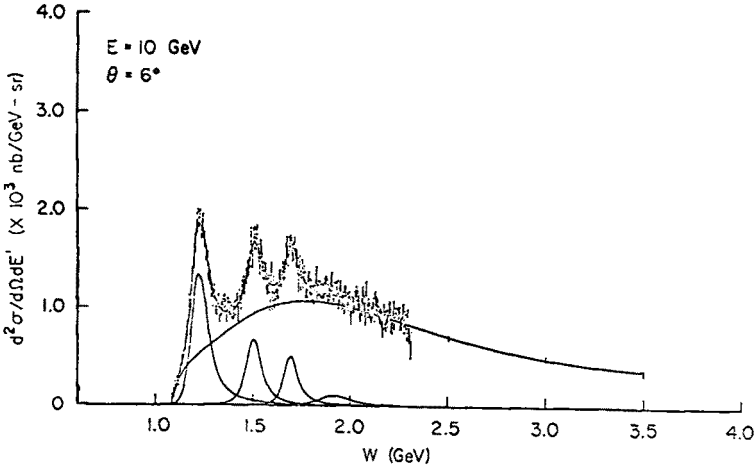

Fig. 2. Same as Fig. 1 at $\varepsilon_1 = 10$ GeV [4]

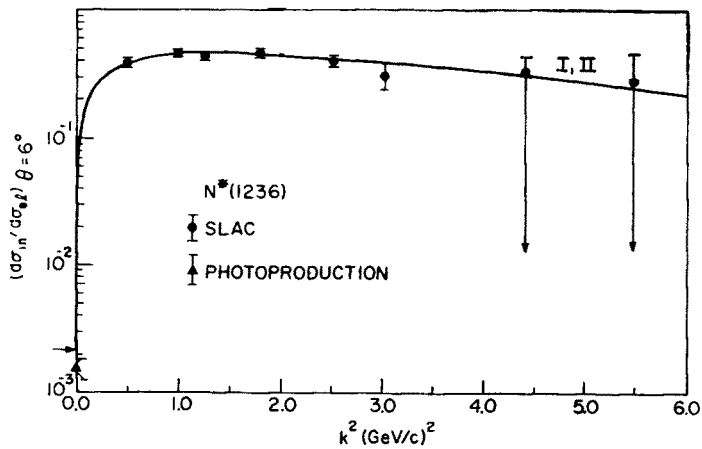

Fig. 3. $d\sigma_{\text{in}}/d\sigma_{\text{el}}$ (see text) at 6° for the 3/2+, 3/2 (1236) resonance. Experimental points are from SLAC Group A[3] and the resonance analysis of Breindenbach [4]. The predictions of models I and II (defined in the text) are indicated [10, 11, 13, 14]

to the excitation of resonant states of the target. The SLAC group has fit their data in this region with a smooth polynomial background term and a series of Breit-Wigner resonance terms whose positions, widths, and strengths were treated as variables. The best resonance fits are also shown in Figures 1 and 2 [3, 4]. The area under the resonance peaks yields the inelastic resonance cross-section

$$\frac{d\sigma_{\text{in}}}{d\Omega_2} = \int_{\text{over resonance}} \left[\frac{d^2\sigma}{d\Omega_2 d\varepsilon_2}\right]_{\varepsilon_1,\theta} d\varepsilon_2 . \tag{1.7}$$

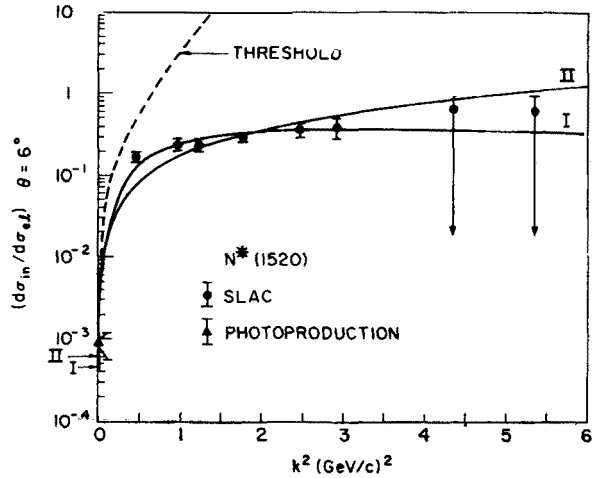

Fig. 4. Same as Fig. 3 for the 1520 MeV resonance region. Also shown is the pure threshold behaviour (Eq. (1.27))

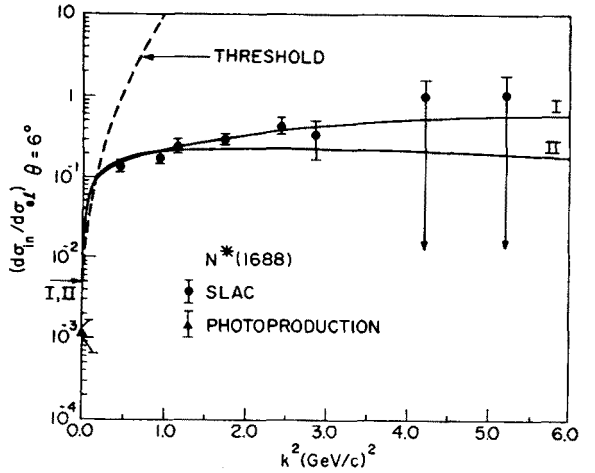

Fig. 5. Same as Fig. 4 for the 1688 MeV resonance region

Figures 3–6 present the ratio $(d\sigma_{in}/d\sigma_{el})_{\theta=6^\circ}$ for the four observed resonances[2]. The experimental points are taken from the analysis of the SLAC data by Breidenbach [4]. The SLAC group has not yet separated the two contributions in Eq. (1.5). On each plot we have

[2] Note

$$\frac{d\sigma_{el}}{d\Omega_2} = \frac{\alpha^2 \cos^2 \frac{\theta}{2}}{4\varepsilon_1^2 \sin^4 \frac{\theta}{2}} \frac{1}{1 + \frac{2\varepsilon_1}{m} \sin^2 \frac{\theta}{2}} \left\{ \frac{G_{E_p}^2 + \frac{\kappa^2}{4m^2} G_{M_p}^2}{1 + \frac{\kappa^2}{4m^2}} + \frac{\kappa^2}{2m^2} G_{M_p}^2 \tan^2 \frac{\theta}{2} \right\}$$

In Figs 3–6 $d\sigma_{el}$ is evaluated at the same ε_1 and θ; however, all the momentum transfer inside the brackets are evaluated at a κ^2 corresponding to the resonance rather than the elastic peak. The resulting ratios (see Eq. (1.18)) are essentially independent of θ for small θ and all the $\kappa^2 \neq 0$ points in Figs 3–6.

one point at $\kappa^2 = 0$ coming from the photoabsorption cross-section integrated over the resonance (see Eqs (1.18) and (1.19)). The qualitative behavior of this ratio for the four peaks is remarkably similar. There is a threshold region where the ratio $(d\sigma_{in}/d\sigma_{el})$ increases rapidly. It then levels off and remains remarkably flat. In addition, the levelling-off value is rather surprisingly close to one in all four cases. The purpose of the present set of lectures is to seek a theoretical understanding of the electroproduction of nucleon resonances.

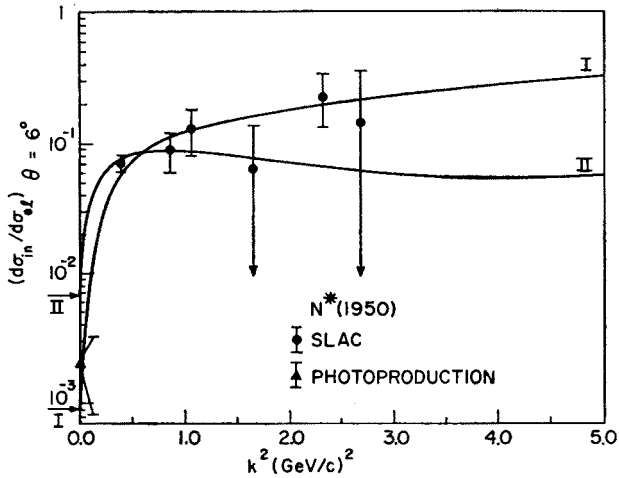

Fig. 6. Same as Fig. 3 for the 1950 MeV resonance region

We start our discussion with a general analysis of the process of excitation of a discrete state (or isobar) of mass M and spin-parity J^{π_R}[5, 6]. We know from

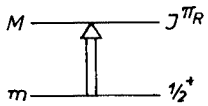

electron excitation of nuclei that a $1/2^+ \to J^{\pi_R}$ transition can take place through one coulomb, one transverse electric, and one transverse magnetic multipole (except for a $1/2^+ \to \to 1/2^\pm$ transition where only one of the transverse terms contributes) and therefore we expect the relativistic vertex to be characterized by three (two for $1/2^+ \to 1/2^\pm$) independent amplitudes or inelastic form factors.

If the final state of the target has a definite mass, we can write for this state

$$W_{\mu\nu} = \frac{d\boldsymbol{P}'}{E'} \delta^{(4)}(P - P' - \kappa) m^2 T_{\mu\nu} \tag{1.8}$$

where the covariant tensor $T_{\mu\nu}$ has the same form as in Eq. (1.4) and may be evaluated in the isobar rest frame as

$$T_{\mu\nu} = \frac{1}{2} \sum_{\lambda} \sum_{\mathcal{M}} \langle \boldsymbol{\kappa}^* \lambda | \hat{J}_\nu(0) | J^{\pi_R} \mathcal{M} \rangle \langle \hat{J}^{\pi_R} \mathcal{M} | \hat{J}_\mu(0) | \boldsymbol{\kappa}^* \lambda \rangle \left(\frac{EE'\Omega^2}{m^2} \right). \tag{1.9}$$

In this expression $\kappa \equiv (\boldsymbol{\kappa}^*, i\kappa_0)$, λ is the initial proton helicity, and $J^{\pi_R}\mathscr{M}$ are the angular momentum, parity, and z-component of the angular momentum of the isobar. Using the results of Jacob and Wick [7], the proton helicity states can be superposed to give eigenstates of angular momentum according to

$$|\kappa jm\lambda\rangle = \left(\frac{2j+1}{4\pi}\right)^{1/2} \int d\Omega_\kappa \mathscr{D}^j_{m\lambda}(-\varphi_\kappa, -\theta_\kappa, \varphi_\kappa)^* |\boldsymbol{\kappa}\lambda\rangle \tag{1.10}$$

where $\mathscr{D}^j_{m\lambda}$ are the familiar rotation matrices [8]. Inverting this relation through the completeness of the $\mathscr{D}$'s we have

$$|\boldsymbol{\kappa}\lambda\rangle = \sum_{jm} \left(\frac{2j+1}{4\pi}\right)^{1/2} \mathscr{D}^j_{m\lambda}(-\varphi_\kappa, -\theta_\kappa, \varphi_\kappa)|\kappa jm\lambda\rangle. \tag{1.11}$$

The problem is therefore reduced to examining matrix elements of the form

$$\langle J^{\pi_R}\mathscr{M}|\hat{J}_\mu(0)|\boldsymbol{\kappa}^*\lambda\rangle = \sum_{jm} \left(\frac{2j+1}{4\pi}\right)^{1/2} \mathscr{D}^j_{m\lambda}(-\varphi_\kappa, -\theta_\kappa, \varphi_\kappa)\langle J^{\pi_R}\mathscr{M}|\hat{J}_\mu(0)|\kappa jm\lambda\rangle. \tag{1.12}$$

For $\hat{\boldsymbol{J}}(0)$, the Wigner-Eckart theorem implies $j = J, J\pm 1$, while for $\hat{J}_0(0)$ it states $J = j$. There is, however, one relation between these four reduced matrix elements coming from current conservation

$$\kappa_\mu \langle J^{\pi_R}\mathscr{M}|\hat{J}_\mu(0)|\boldsymbol{\kappa}^*\lambda\rangle = 0 \tag{1.13}$$

and the problem is thus reduced to three independent amplitudes, or inelastic form factors, in accordance with our above discussion.

In defining the inelastic form factors it is first convenient to introduce linear combinations of helicity states corresponding to parity eigenstates [6, 7]

$$|\kappa, \pi = \pm 1, jm\rangle = \frac{1}{\sqrt{2}}\left[|\kappa jm\tfrac{1}{2}\rangle \pm (-1)^{j-1/2}|\kappa jm-\tfrac{1}{2}\rangle\right] \tag{1.14}$$

and linear combinations of reduced matrix elements [6]

$$f_\varrho \equiv \sum_j \left(\frac{2j+1}{2J+1}\right)^{1/2} \langle j\tfrac{1}{2}1\varrho|j1J\tfrac{1}{2}+\varrho\rangle \langle J^{\pi_R}\|\hat{\boldsymbol{J}}(0)\|\kappa^*\pi j\rangle \left(\frac{EE'\Omega^2}{8\pi M^2}\right)^{1/2} \tag{1.15a}$$

with $\varrho = 0, \pm 1$ (denoted $0, \pm$) and[3]

$$f_c \equiv -\langle J^{\pi_R}\|\hat{J}_0(0)\|\kappa^*\pi J\rangle \left(\frac{EE'\Omega^2}{8\pi M^2}\right)^{1/2}. \tag{1.15b}$$

[3] For convenience, a minus sign has been included here in the definition of f_c.

The continuity equation then simplifies to

$$f_0 = -\frac{\kappa_0}{\kappa^*} f_c. \tag{1.16}$$

The components of $T_{\mu\nu}$ in the isobar rest frame yield, after a little algebra, two relations

$$\sum_{i=1}^{3} T_{ii} = \sum_j |\langle J^{\pi_R}||\hat{J}(0)||\kappa^*\pi j\rangle|^2 \left(\frac{EE'\Omega^2}{8\pi m^2}\right) = \frac{M^2}{m^2}\sum_e |f_e|^2. \tag{1.17}$$

(Equation (1.17) continued)

$$T_{44} = -|\langle J^{\pi_R}||\hat{J}_0(0)||\kappa^*\pi J\rangle|^2 \left(\frac{EE'\Omega^2}{8\pi m^2}\right) = -\frac{M^2}{m^2}|f_c|^2$$

which can be used to determine $T_{1,2}(\kappa^2)$ and the electron scattering cross-section in the lab becomes [6]

$$\left(\frac{d\sigma}{d\Omega}\right)_{\text{lab}} = \frac{\alpha^2\cos^2\frac{\theta}{2}}{4\varepsilon_1^2\sin^4\frac{\theta}{2}} \cdot \frac{1}{1+\frac{2\varepsilon_1}{m}\sin^2\frac{\theta}{2}}\left[\frac{\kappa^4}{\kappa^{*4}}|f_c|^2 + \left(\frac{\kappa^2}{2\kappa^{*2}} + \right.\right.$$

$$\left.\left. + \frac{M^2}{m^2}\tan^2\frac{\theta}{2}\right)(|f_+|^2+|f_-|^2)\right]. \tag{1.18}$$

The photoabsorption cross-section for excitation of the isobar can also be immediately obtained as [6]

$$\int_{\text{lab; over resonance}} \sigma_\gamma(\omega)d\omega = \frac{4\pi^2\alpha}{M^2-m^2}\cdot\frac{M^2}{m}(|f_+|^2+|f_-|^2)_{\kappa^2=0}. \tag{1.19}$$

Equations (1.18) and (1.19) are the main results of this section. The problem is now reduced to a set of inelastic form factors. A few properties of these form factors follow from general principles. For example, the entire κ^* dependence of the reduced matrix elements is contained in the nuclear state vectors $|\kappa^*\lambda\rangle$. An explicit construction of this state can be given by noting that there is a unitary operator $e^{\Omega\hat{K}_z}$ which boosts a particle from rest to a momentum κ^* in the z direction

$$|\kappa^*\lambda\rangle = e^{\Omega\hat{K}_z}|0\lambda\rangle$$

$$\Omega = \tanh^{-1}\frac{\kappa^*}{(\kappa^{*2}+m^2)^{1/2}} \underset{\kappa^*\to 0}{\to} \frac{\kappa^*}{m}. \tag{1.20}$$

The operator $\hat{K}_z$ which generates the Lorentz transformation in the z direction is a polar-vector operator under spatial rotations and reflections. It follows from Eq. (1.10) that

$$|\kappa^* jm\lambda\rangle = \left(\frac{2j+1}{4\pi}\right)^{1/2} \int d\Omega_\kappa \mathscr{D}^j_{m\lambda}(-\varphi_\kappa, -\theta_\kappa, \varphi_\kappa)^* \hat{R}_{-\varphi_\kappa - \theta_\kappa \varphi_\kappa} e^{\Omega \hat{K}_z} |0\lambda\rangle \tag{1.21}$$

where

$$\hat{R}_{\alpha\beta\gamma} = e^{i\alpha \hat{J}_z} e^{i\beta \hat{J}_y} e^{i\gamma \hat{J}_z} \tag{1.22}$$

is the finite rotation operator. If we now let $\kappa^* \to 0$, we observe that $\hat{K}_z$ must act often enough in the expansion of the exponential to obtain a basis for the j^{th} representation of the rotation group. Otherwise, the integrations over $\mathscr{D}^{j*}_{m\lambda}$ give zero. Furthermore, since $\hat{K}_z$ is a polar vector, it must act often enough to yield a state of the correct parity, which is what we eventually want. Since each time a $\hat{K}_z$ acts, it carries with it a power of (κ^*/m), the κ^* dependence can be read off in the various cases [5, 6]

i) Normal-parity transitions: $1/2^+ \to 3/2^-, 5/2^+, 7/2^-$, *etc.*

$$f_c \sim (\kappa^*)^{J-1/2}$$
$$f_\pm \sim (\kappa^*)^{J-3/2} \tag{1.23}$$

ii) Abnormal-parity transitions: $1/2^+ \to 1/2^-, 3/2^+, 5/2^-$, *etc.*

$$f_c \sim (\kappa^*)^{J+1/2}$$
$$f_\pm \sim (\kappa^*)^{J-1/2}. \tag{1.24}$$

In the case $1/2^- \to 1/2^\pm$, Eq. (1.15a) implies that $f_\perp \equiv 0$ and there are only two form factors. Furthermore, in the case of $1/2^+ \to 1/2^+$ transitions, the $\kappa^* \to 0$ limit of the electric monopole operator is just 1, the total charge, and cannot cause transitions. Therefore, the threshold behavior in this case is $f_c \sim (\kappa^*)^2, f_- \sim \kappa^*$.

One might be tempted to conclude from these arguments that the expansion parameter for threshold behavior is κ^*/m. However, this argument is invalid since, at least in nuclear physics, it is known that the relevant quantity is the size of the target and not the reciprocal of its mass.

Since the four-momentum transfer must be space-like, $\kappa^2 \geq 0$, there is a minimum three-momentum transfer

$$\kappa^* \geqslant \frac{m+M}{2M}(M-m) \tag{1.25}$$

for electroproduction of an isobar of mass M. Thus it is not clear *a priori* whether the above threshold relations have any applicability in the experimentally accessible region.

In the case of normal-parity transitions, the threshold conditions (1.23) can be combined with the continuity equation (1.16) and the definitions (1.15) to yield the relation [6]

$$\frac{|f_+|^2 + |f_-|^2}{|f_c|^2} \underset{\kappa^* \to 0}{\to} \left(\frac{\kappa_0}{\kappa^*}\right)^2 \frac{J+\frac{1}{2}}{J-\frac{1}{2}} \qquad J \geqslant \tfrac{3}{2}. \tag{1.26}$$

This relation is familiar in nuclear physics and is just that used to relate the lifetime for photon processes to coulomb excitation. Thus we can combine Eqs (1.23) and (1.26) to write a "threshold cross-section", which follows from very general grounds, for $1/2^+ \to 3/2^-$ $5/2^+$, $7/2^-$, *etc.* normal-parity transitions [6]

$$\left(\frac{d\sigma}{d\Omega}\right)_{\text{thresh}} = \frac{\alpha^2 \cos^2 \frac{\theta}{2}}{4\varepsilon_1^2 \sin^4 \frac{\theta}{2}} \cdot \frac{1}{1 + \frac{2\varepsilon_1}{m} \sin^2 \frac{\theta}{2}} \left\{ \frac{\kappa^4}{\kappa^{*4}} + \right.$$

$$\left. + \left(\frac{\kappa_0}{\kappa^*}\right)^2 \left(\frac{J+\frac{1}{2}}{J-\frac{1}{2}}\right) \left(\frac{\kappa^2}{2\kappa^{*2}} + \frac{M^2}{m^2} \tan^2 \frac{\theta}{2}\right) \right\} |a_J^c|^2 (\kappa^*)^{2J-1} \tag{1.27}$$

where a_J^c is a constant. The results obtained using this threshold cross-section normalized to photoproduction are shown in Figs 4 and 5. While it does provide a good description of $(d\sigma_{\text{in}}/d\sigma_{\text{el}})$ for very small κ^2, the experimental data soon fall away from the threshold curve, indicating that the internal structure of the target is then playing an important role.

The analytic properties of the inelastic form factors are discussed in Ref. [6]. They are more complicated than in the elastic case, with complex anomolous thresholds being present. So far the analytic properties of these objects have not proven very useful.

In the next lecture we shall discuss the nucleon isobars as resonances in pion electroproduction

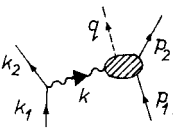

$$W^2 = -(p_1 + k)^2$$
$$k \equiv -\varkappa = k_1 - k_2$$
$$\Delta = \tfrac{1}{2}(k - q)$$

The invariant amplitude for this process can be expanded in terms of six independent kinematic invariants M_i^μ, $i = 1, \ldots, 6$ [for example, $M_1^\mu \varepsilon^\mu = \frac{i}{2} \gamma_5 (\not{\varepsilon}\not{k} - \not{k}\not{\varepsilon})$] [9]

$$\left(\frac{2\omega_q E_1 E_2 \Omega^3}{m^2}\right)^{1/2} \langle q p_2^{(-)} | \hat{J}_\mu \varepsilon_\mu | p_1 \rangle =$$

$$= \bar{u}(p_2) \left[\sum_{i=1}^{6} \varepsilon_\mu M_i^\mu A_i(W, \Delta^2, k^2) \right] u(p_1) \equiv \varepsilon_\mu J_\mu \tag{1.28}$$

which explicitly satisfy current conservation.

$$k_\mu M_i^\mu = 0 \quad i = 1, \ldots, 6. \tag{1.29}$$

In this expression ε_μ is the Møller potential coming from the electron part of the diagram.

$$\varepsilon_\mu = \frac{1}{k^2} \bar{u}(k_2) \gamma_\mu u(k_1). \tag{1.30}$$

---

[4] Here and henceforth we take the Dirac wavefunctions to be normalized to $\bar{u}u = 1$.

The expression (1.28) can be decomposed into helicity amplitudes in the CM system where $\boldsymbol{p}_1 = -\boldsymbol{k}^*$ defines the z direction according to [10]

$$\frac{m}{4\pi W}\, \boldsymbol{J}\cdot \boldsymbol{e}_{k,\lambda_k} \equiv$$

$$\equiv \frac{1}{(4k^*q)^{1/2}} \sum_J (2J+1)\mathscr{D}^J_{\lambda_1-\lambda_k,\lambda_2}(-\varphi_p, -\theta_p, \varphi_p)\, \langle \lambda_2 | T^J(W, k^2) | \lambda_1, \lambda_k \rangle \qquad (1.31)$$

where the angles refer to $\boldsymbol{p}_2$ and

$$e_{k,\pm 1} \equiv \mp \frac{1}{\sqrt{2}} (e_{k,1} \pm i e_{k,2}) \qquad (1.32)$$

$$e_{k,0} \equiv \boldsymbol{k}/|\boldsymbol{k}|$$

are the familiar helicity unit vectors. (This helicity analysis can be immediately generalized to any two-particle final state of the target.) The matrix elements J_0 can be obtained from current conservation. The above analysis, including the relations between the invariant amplitudes A_i and the helicity amplitudes, is carried out in detail in Ref. [10–12] and will not be reproduced here. The main point for us here is that the inelastic form factors can be simply expressed in terms of the helicity amplitudes in Eq. (1.31) [10–13]

$$|f_c|^2 = \frac{J+{}^1\!/_2}{k^*} \int_{\text{res}} |\langle \tfrac{1}{2}^{\pm} | T^J(W, k^2) | \tfrac{1}{2}^{\pm}, 0 \rangle|^2 dW$$

$$|f_+|^2 + |f_-|^2 = \frac{J+{}^1\!/_2}{k^*} \int_{\text{res}} [|\langle \tfrac{1}{2}^{\pm} | T^J(W, k^2) | \tfrac{3}{2}^{\pm}, 1 \rangle|^2 +$$

$$+ |\langle \tfrac{1}{2}^{\pm} | T^J(W, k^2) | \tfrac{1}{2}^{\pm}, 1 \rangle|^2] dW \qquad (1.33)$$

where we have introduced the appropriate linear combinations of helicity states to give parity eigenstates and the states are now characterized by $\pi = (-1)^{J \pm 1/2}$, $\lambda = |\lambda_a - \lambda_b|$, and $|\lambda_k|$.

At this point we have essentially exhausted the general properties of the process. To proceed further we must introduce some further information about the target, and in the next two lectures we will discuss the consequences of two very simple models of the nucleon.

2. A relativistic model

A. Elastic resonances in pion electroproduction
   i) Model and justification
   ii) As approximate solution to Omnès equation
B. Extension to inelastic resonances

C. A coupled-channel calculation
   i) One resonant eigenphase shift
   ii) The subtraction point
   iii) Recovery of previous results
D. The excitation mechanism
   i) $|\pi N\rangle$ channel
   ii) $|\pi N^*(1236)\rangle$ channel
E. Comparison with experiment
   i) Resonance spectrum
   ii) Inelastic form factors
F. Coincidence experiments

In this lecture isobar formation is viewed as a resonance in pion electroproduction and we start with the case where the resonance can only decay elastically back into the $|\pi N\rangle$ channel. The three independent helicity amplitudes in Eq. (1.33) shall be denoted generically by $a(W, k^2)$. The model then consists of writing [10, 11]

$$a(W, k^2) = a^{\text{lhs}}(W, k^2)/D(W) \tag{2.1}$$

where $a^{\text{lhs}}(W, k^2)$ is the multipole projection of a gauge-invariant set of exchange graphs thought to play an important role in the excitation, and $D(W)$ is a final-state enhancement factor. For example, there is an expression due to Watson [15]

$$D(W) = \exp\left[-\frac{1}{\pi}\int_{W_0}^{\infty} dW' \frac{\delta(W')}{W' - W - i\varepsilon}\right] \tag{2.2}$$

where $W_0 = m + \mu$ is the $|\pi N\rangle$ threshold and $\delta(W)$ is the $|\pi N\rangle$ scattering phase shift in the appropriate channel. The process

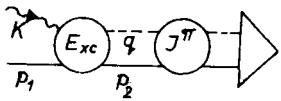

can thus be considered as proceeding in two steps. First, there is an excitation amplitude to produce the $|\pi N\rangle$ system in the appropriate J^π state, and then, once the system is produced, there is a resonance mechanism, which need not be specified at this point, that builds up the resonance. The model may be justified on the following grounds:

i) The calculation is completely gauge invariant and covariant.

ii) The amplitude has the correct threshold behaviors in k^* and q since the multipole projection of any Feynman amplitude has these properties.

iii) The amplitude has the correct analytic properties since $a^{\text{lhs}}(W, k^2)$ has left-hand-singularities (lhs) located at the correct places while $D(W)$ has the right-hand unitarity cut (rhc) in W. Note that we will only have a model of the lhs region, however.

iv) The amplitude (2.1) satisfies the final-state theorem coming from unitarity and time reversal since on the rhc, $a^{\text{lhs}}(W, k^2)$ is real and

$$D(W) = \left|D(W)\right| e^{-i\delta(W)} \; W \geqslant W_0. \tag{2.3}$$

v) The model represents an approximate solution to the Omnès equation in the vicinity of a resonance provided that $a^{\text{lhs}}(W, k^2)$ is a slowly varying function of W in the region where $\sin \delta(W) \neq 0$ on the rhc.

vi) The electroproduction amplitude now resonates at the same place as does elastic scattering. To see this, we define a resonance by (compare Eq. (2.3))

$$\text{Re } D(W_R) = 0 \tag{2.4}$$

$D(W)$ can then be expanded in the vicinity of the resonance as

$$D(W) \cong (W - W_R)\left[\frac{d}{dW} \text{Re } D(W)\right]_{W_R} + i \text{ Im } D(W_R) \equiv$$

$$\equiv \text{Re}' D(W_R)\,[W - W_R + i\Gamma/2] \tag{2.5}$$

where it is assumed that Im $D(W)$ is slowly varying. This leads to the familiar Breit-Wigner form for $a(W, k^2)$, and the inelastic form factors (see Eq. (1.33)) are given by

$$\int\limits_{\text{resonance}} \left|a(W, k^2)\right|^2 dW \cong \frac{2\pi}{\Gamma}\left|\frac{a^{\text{lhs}}(W_R, k^2)}{\text{Re}' D(W_R)}\right|^2. \tag{2.6}$$

Before continuing the discussion of the model, we present a demonstration of point *v*) above [10, 11]. Since the phase of $a(W, k^2)$ on the rhs is assumed known from the final-state theorem, $a(W, k^2)$ satisfies an Omnès equation [16]

$$a(W, k^2) = a^{\text{lhs}}(W, k^2) + \frac{1}{\pi}\int\limits_{W_0}^{\infty} \frac{e^{-i\delta(W')} \sin \delta(W') a(W', k^2) dW'}{W' - W - i\varepsilon} \tag{2.7}$$

$$W_0 \leqslant W \leqslant \infty$$

where it has been assumed that $a^{\text{lhs}}(W, k^2)$ is given in the region $W_0 \leqslant W \leqslant \infty$. A solution to this singular integral equation was obtained by Omnès [16]

$$a(W, k^2) = e^{i\delta(W)}\left[a^{\text{lhs}}(W, k^2) \cos \delta(W) + \right.$$

$$\left. + e^{\varrho(W)} \frac{\mathscr{P}}{\pi}\int\limits_{W_0}^{\infty} \frac{a^{\text{lhs}}(\xi, k^2) \sin \delta(\xi) e^{-\varrho(\xi)} d\xi}{\xi - W}\right] \tag{2.8}$$

where

$$\varrho(W) \equiv \frac{\mathscr{P}}{\pi}\int\limits_{W_0}^{\infty} d\zeta \frac{\delta(\zeta)}{\zeta - W}. \tag{2.9}$$

(All integrals will be assumed to converge as written for the purposes of the present simplified discussion.) Now if $a^{\text{lhs}}(W, k^2)$ is slowly varying where $\sin\delta(W) \neq 0$, then in the vicinity of the resonance

$$a(W, k^2) \cong a^{\text{lhs}}(W, k^2)\chi(W) \tag{2.10}$$

where

$$\chi(W) = \exp\left[\frac{1}{\pi}\int_{W_0}^{\infty}\frac{\delta(W')dW'}{W'-W-i\varepsilon}\right]\psi(W) \tag{2.11}$$

and

$$\psi(W) = \exp\left[-\frac{1}{\pi}\int_{W_0}^{\infty}\frac{\delta(W')dW'}{W'-W-i\varepsilon}\right] + \\ + \frac{1}{\pi}\int_{W_0}^{\infty}d\xi\,\frac{\sin\delta(\xi)}{\xi-W-i\varepsilon}\exp\left[-\frac{\mathscr{P}}{\pi}\int_{W_0}^{\infty}\frac{\delta(\zeta)d\zeta}{\zeta-\xi}\right]. \tag{2.12}$$

We have factored out $a^{\text{lhs}}(W, k^2)$ and then subtracted and added $i\sin\delta(W)$ in the bracketed expression in Eq. (2.8). Now, by inspection, $\psi(W)$ has the following properties:

i) $\psi(W)$ is analytic in the W plane with only a rhc for $W_0 \leq W \leq \infty$.

ii) $\psi(W) \to 1$ as $|W| \to \infty$.

An unsubtracted dispersion relation can therefore be written for $\psi(W)-1$

$$\psi(W)-1 = \frac{1}{\pi}\int_{W_0}^{\infty}\frac{\text{disc}\,\psi(W')dW'}{W'-W-i\varepsilon} \tag{2.13}$$

but on the cut

$$\text{disc}\,\psi(W) = \exp\left[-\frac{\mathscr{P}}{\pi}\int_{W_0}^{\infty}\frac{\delta(\zeta)d\zeta}{\zeta-W}\right][-\sin\delta(W)+\sin\delta(W)] = 0. \tag{2.14}$$

Hence

$$\psi(W) = 1 \tag{2.15}$$

and Eqs (2.10), (2.11) reduce to Eqs (2.1), (2.2) which is the desired result.

If it is assumed that at some point $W = m_s$, $a(m_s, k^2) \cong a^{\text{lhs}}(m_s, k^2)$, then $D(W)$ may be subtracted at this point

$$D(W) = \exp\left[-\frac{W-m_s}{\pi}\int_{W_0}^{\infty}dW'\,\frac{\delta(W')}{(W'-m_s)(W'-W-i\varepsilon)}\right]. \tag{2.16a}$$

$$D(m_s) = 1. \tag{2.16b}$$

The above discussion makes rather strong assumptions about the behavior of $\sin\delta(W)$ and convergence of the integrals involved. In any event, the model given by Eqs (2.1),

(2.2) or (2.1), (2.16) will be assumed to have a more general validity than this demonstration might imply.

This discussion can be considered as a simplified synthesis and summary of some very detailed work on the first nucleon resonance, $3/2^+$, 3/2(1236) by Fubini, Nambu, and Wataghin [9], Dennery [17], Zagury [18], Gutbrod and Simon [19], Vik [20] and Adler [21]. Our aim is to extend these ideas to the higher nucleon resonances.

Unfortunately, unlike the $N^*(1236)$ which decays elastically, the higher resonances can decay into other channels, and the previous analysis must be extended to inelastic resonances. The simplest way to do this is to write [10]

$$f(W) \equiv \frac{e^{i\delta}\sin\delta}{q} = N(W)/D(W) \tag{2.17}$$

where $f(W)$ is the partial-wave amplitude for $|\pi N\rangle$ scattering satisfying general inelastic unitarity

$$\mathrm{Im}\,\frac{1}{f} = -q\,\frac{\sigma_{\mathrm{tot}}}{\sigma_{\mathrm{el}}} \equiv -q\,\frac{\Gamma}{\Gamma_{\mathrm{el}}} \tag{2.18}$$

with all quantities referring to the J^π channel. In Eq. (2.17), $N(W)$ is assumed to have only left-hand singularities and $D(W)$ to have the right-hand unitarity cut. We may then again make the model (2.1) for $|\pi N\rangle$ electroproduction, only now we use the $D(W)$ in Eq. (2.17). A resonance in $|\pi N\rangle$ electroproduction can still be defined by Eqs (2.4), (2.5), and in this case $f(W)$ assumes the familiar Breit-Wigner form

$$f(W) = \frac{-\Gamma_{\mathrm{el}}/2q}{W - W_R + i\Gamma/2} \tag{2.19}$$

where use has been made of the inelastic unitarity condition (2.18), and

$$\int_{\text{resonance}} |a(W, k^2)|^2_{\gamma^*+N\to N+\pi} dW \cong \frac{2\pi}{\Gamma}\left|\frac{a^{\mathrm{lhs}}(W_R, k^2)}{\mathrm{Re}'\, D(W_R)}\right|^2. \tag{2.20}$$

This is now a model for the process $\gamma^*+N\to N+\pi$ through the resonance. In the "compound-nucleon" picture, the decay of a sharp resonance is independent of the mode of formation. Therefore, to get the probability for $\gamma^*+N\to$ anything, we simply multiply the above by $\Gamma/\Gamma_{\mathrm{el}}$

$$\int_{\text{resonance}} |a(W, k^2)|^2_{\gamma^*+N\to\text{anything}} dW \cong \frac{2\pi}{\Gamma}\left|\frac{a^{\mathrm{lhs}}(W_R, k^2)}{\mathrm{Re}'\, D(W_R)}\right|^2 \frac{\Gamma}{\Gamma_{\mathrm{el}}}. \tag{2.21}$$

We shall refer to this as model I. Note that the k^2 dependence in Eq. (2.21) is explicit in the expression $|a^{\mathrm{lhs}}(W_R, k^2)|^2$. While this result has the advantage of simplicity, it is somewhat unsatisfactory since if a resonance can decay inelastically, it must also be

possible to form the resonance inelastically. To improve this result, we therefore turn to a coupled-channel calculation [11].

We assume that the resonance can be formed through

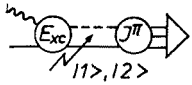

two channels $|1\rangle$ and $|2\rangle$, which shall actually be taken as $|\pi N\rangle$ and $|\pi N^*(1236)\rangle$ (lowest l value) in the subsequent calculations. Now the strong-interaction two-channel S-matrix for a given J^π is unitary and symmetric and can always be diagonalized with a real rotation. Thus if we define

$$|e_i\rangle = \sum_{j=1}^{2} R_{ij}|j\rangle \tag{2.22}$$

with

$$\underline{R} = \begin{pmatrix} \cos\varepsilon & \sin\varepsilon \\ -\sin\varepsilon & \cos\varepsilon \end{pmatrix}$$

then

$$\underline{S}_e = \underline{R}\underline{S}\underline{R}^{-1} = \begin{pmatrix} e^{2i\xi_1} & 0 \\ 0 & e^{2i\xi_2} \end{pmatrix} \tag{2.24}$$

where the eigenphase shifts $\xi_{1,2}$ are real. As the simplest model of an inelastic resonance [22] we assume that one eigenphase shift $\xi_1 \equiv \xi$ is resonant

$$e^{i\xi}\sin\xi = \frac{-\Gamma/2}{W - W_R + i\Gamma/2} \tag{2.25}$$

and for the other

$$\sin\xi_2 \cong 0. \tag{2.26}$$

The strong-interaction T-matrix then takes the form

$$\underline{T} \equiv \frac{1}{2i}(\underline{S}-\underline{1}) = e^{i\xi}\sin\xi \begin{pmatrix} \cos^2\varepsilon & \cos\varepsilon\sin\varepsilon \\ \cos\varepsilon\sin\varepsilon & \sin^2\varepsilon \end{pmatrix}. \tag{2.27}$$

The scattering amplitude in channel $|1\rangle$ can therefore be identified as

$$\frac{1}{2i}(e^{2i\delta_1} - 1) = (\cos^2\varepsilon)e^{i\xi}\sin\xi \tag{2.28}$$

which allows an evaluation of both ξ and $|\varepsilon|$ from the experimental (complex) values of δ_1[5]. It also follows from Eq. (2.27) that at resonance, the branching ratios into channels $|1\rangle$ and $|2\rangle$ are given by

$$\Gamma_1/\Gamma = \cos^2\varepsilon$$
$$\Gamma_2/\Gamma = \sin^2\varepsilon. \tag{2.29}$$

[5]The choice of sign ε is discussed in Ref. [11].

Since the resonant eigenchannel is now

$$|e_1\rangle = \cos\varepsilon\,|1\rangle + \sin\varepsilon\,|2\rangle \tag{2.30}$$

the previous model can be easily extended to give

$$A_1(W, k^2) = [a_1^{\text{lhs}}(W, k^2)\cos\varepsilon + a_2^{\text{lhs}}(W, k^2)\sin\varepsilon]/D(W) \tag{2.31}$$

$$D(W) = \exp\left[-\frac{1}{\pi}\int_{W_0}^{\infty} dW'\,\frac{\xi(W')}{W'-W-i\varepsilon}\right]. \tag{2.32}$$

The eigenchannel $|e_l\rangle$ is first produced with the amplitude $a_1^{\text{lhs}}\cos\varepsilon + a_2^{\text{lhs}}\sin\varepsilon$, and the resonance mechanism then builds up the final-state enhancement factor $D(W)$ which now involves an integral over the real eigenphase shift. The simplifying assumptions that we have made have reduced the two-channel problem back to a single resonant channel. In electroproduction, the inelastic form factors are given by (compare Eq. (1.33))

$$\int_{\text{resonance}} |A_1(W, k^2)|^2 dW \cong$$

$$\cong \frac{2\pi}{\Gamma}\left|[a_1^{\text{lhs}}(W_R, k^2)\cos\varepsilon_R + a_2^{\text{lhs}}(W_R, k^2)\sin\varepsilon_R]/\text{Re}'\,D(W_R)\right|^2 =$$

$$= \int_{\text{res}} |a_1(W, k^2)|^2 dW + \int_{\text{res}} |a_2(W, k^2)|^2 dW\,. \tag{2.33}$$

An analysis of the experimental $|\pi N\rangle$ scattering data indicates that $\xi \underset{W\to\infty}{\to} \pi/2$ for all the resonances we are interested in [11, 14]. Thus we are forced to perform a subtraction in Eq. (2.32) and write

$$D(W) = \exp\left[-\frac{W-m_s}{\pi}\int_{W_0}^{\infty} dW'\,\frac{\xi(W')}{(W'-m_s)(W'-W-i\varepsilon)}\right]$$

$$D(m_s) = 1\,. \tag{2.34}$$

This introduces an unknown parameter m_s, equivalent to the absolute strength of the resonance at some point, into our analysis. We shall refer to the present calculation as model II. The results in model I can be recovered in several limiting cases of model II. For example, if $a_1^{\text{lhs}} \cong a_2^{\text{lhs}}$ and $\Gamma_1 \cong \Gamma_2$, then

$$\int_{\text{resonance}} |A_1(W, k^2)|^2 dW \cong \frac{2\pi}{\Gamma}\,\frac{\Gamma}{\Gamma_1}\left|\frac{a_1^{\text{lhs}}(W_R, k^2)}{\text{Re}'\,D(W_R)}\right|^2. \tag{2.35}$$

The next problem is to discuss the excitation amplitudes $a_{1,2}^{\text{lhs}}(W, k^2)$. For the $|\pi N\rangle$ channel we have kept the graphs shown in Fig. 7. These graphs are treated as "generalized Feynman amplitudes" which means they are computed as Feynman graphs using renor-

malized, mass-shell couplings at the vertices. Such amplitudes will properly reproduce all the pole terms in a dispersion theory. It is clear that graphs (b) and (c) involve the elastic nucleon form factors. In order to make the sum of these graphs explicitly gauge invariant, we make the simplifying assumption that $F_\pi(k^2) = F_1^V(k^2)$. This is consistent with existing experiments. In graph (d), only the coupling $ig_{\omega NN}\bar{\psi}\gamma_\mu\psi\omega_\mu$ is retained at the nucleon vertex. The coupling constant $g_{\omega\pi\gamma}$ is known from the decay of the ω. It is the large value of this coupling which motivated us to retain graph (d). Unfortunately,

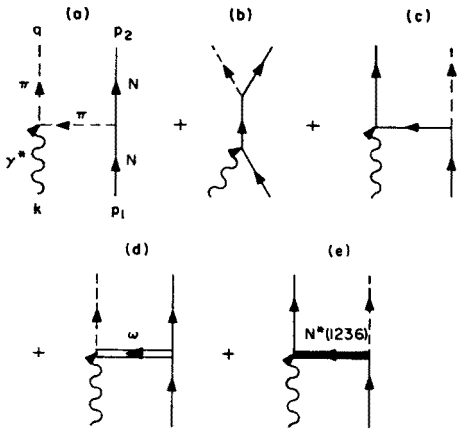

Fig. 7. Generalized Feynman amplitudes used as the excitation mechanism for the $|\pi N\rangle$ channel [10, 11, 13]

the relative sign of these two couplings, which is essential since amplitudes must be added, is unknown. We have therefore taken

$$\beta = -\sqrt{10}\,\frac{g_{\omega\pi\gamma}}{|g_{\omega\pi\gamma}|}\cdot\frac{g_{\omega NN}}{g_{\pi NN}} \tag{2.36}$$

as a parameter and chosen the value $\beta = -6$ to give the best overall fit. The resulting value of $|g_{\omega NN}/g_{\pi NN}|$ is consistent with other measurements of this quantity [10]. The form factor entering in graph (d) is unknown. Based on rather flimsy arguments of vector-meson dominance, it has been taken as

$$F_{\omega\pi\gamma}(k^2) = F_2^V(k^2)/F_2^V(0). \tag{2.37}$$

The last graph (e) (which was only included in model II) involves the inelastic form factor for $N^*(1236)$ production. This was taken from experiment. The sign of the product of coupling constants in (e) relative to that in (b) or (c) can be determined by comparing this isobar model with the CGLN calculation of photoproduction [11, 23].

In the $|\pi N^*(1236)\rangle$ channel, channel $|2\rangle$, the graphs shown in Fig. 8 have been retained. The (πNN^*) coupling is taken of the form $\gamma_{\pi NN^*}\left(\bar{\Psi}_\mu\psi\frac{\partial\varphi}{\partial x_\mu}\right)$ and the gauge term (c) is included since this involves a derivative coupling. The relative signs of the couplings in these graphs are all known from the above analysis. Only the convection current part

of graph (e) has been retained for current conservation, and the form factors in graphs (c) and (e) have been determined by demanding that this model sum of graphs be explicitly gauge invariant. The details of these calculations are contained in Refs [10,11,13].

Because of the subtraction parameter m_s in Eq. (2.34), we are unable to calculate the absolute strength of the inelastic form factors for each resonance. Our approach has been to first normalize the relative contributions of each known nucleon resonance to the values measured in photoproduction. Thus the second nucleon resonance region includes

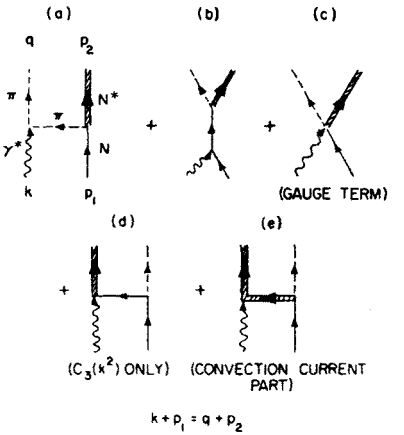

Fig. 8. Same as Fig. 7 for the $|\pi N^*(1236)\rangle$ channel

the $3/2^-$, 1/2 (1525) and $1/2^-$, 1/2 (1550) while the third includes the $5/2^+$, 1/2 (1688); $5/2^-$, 1/2 (1680) − 7%; $1/2^-$, 1/2 (1710); and $1/2^-$, 3/2 (1640). The fourth resonance is assumed to be the $7/2^+$, 3/2 (1950). In the present calculation, the contribution of the $1/2^-$ states remains small at all k^2. Thus the second and third resonances are dominated by the $3/2^-$, 1/2 (1525) and $5/2^+$, 1/2 (1688). The theoretical calculations are then normalized to the SLAC experiments. The values of m_s determined from this normalization are shown in the table. It is

	m_s in GeV	
State	Model I[a]	Model II[b]
$3/2^+$, 3/2 (1236)	0.89[c]	0.86[c]
$3/2^-$, 1/2 (1525)	0.91	1.05
$5/2^-$, 1/2 (1680)	physical region	1.11
$5/2^+$, 1/2 (1688)	0.35	1.13
$7/2^+$, 3/2 (1950)	0.72	0.43

[a] Computed using Eq. (2.35).
[b] Computed using Eq. (2.33).
[c] Computed using Re δ in Eq. (2.16).

interesting to note that the prescription $m_s = m$ gives the absolute normalization for all of the observed resonances to within a factor of 2.

The resonance spectrum calculated from Eqs (2.31), (2.34) at $\varepsilon_1 = 10$ GeV, $\theta = 6°$ is shown in Fig. 9. The eigenphase shifts for the second and third resonances have been determined from the Glasgow phase-shift analysis [14]. Since J^π has not been experimentally measured for the peaks observed in electron scattering, the similarity of the theoretical and experimental resonance spectrum (Figs 2 and 9) at all k^2 is the strongest evidence that we have that we are talking about the correct resonance states.

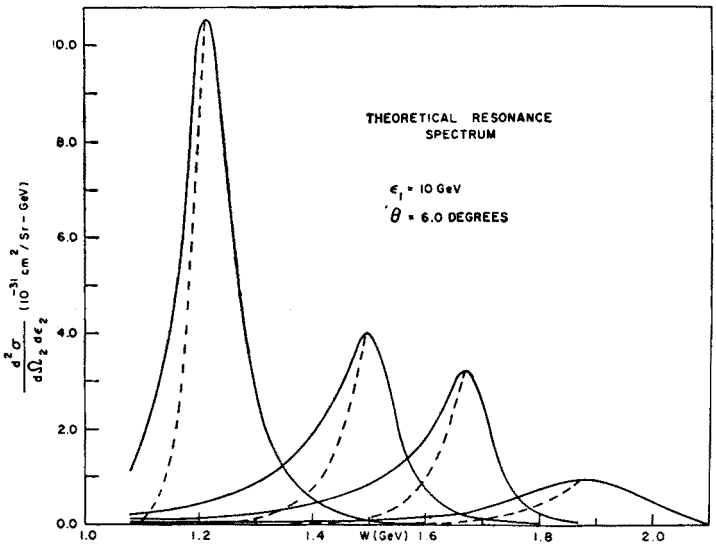

Fig. 9. The resonance spectrum at $\varepsilon_1 = 10$ GeV, $\theta = 6°$ computed from Eqs (2.31), (2.34). This is to be compared with Fig. 2. The eigenphase shifts for the second and third resonances have been determined from the Glasgow phase-shift analysis using Eq. (2.28), for the others the CERN analysis was used [14]. The dashed curves are obtained by multiplying the solid curves with the threshold factor $(q/q_R)^{2l+1}$ below resonance. (This gives some indication of the true behavior near pion threshold) [14]

The theoretical values of $(d\sigma_{\text{in}}/d\sigma_{\text{el}})_{60}$ for the first four nucleon resonances are shown in Figs 3–6 (the calculations based on model I were carried out before the SLAC experiments [10]). The advantage of looking at this ratio is that $G^2_{E_p}(k^2)$ drops out since the inelastic amplitudes in this model are also proportional to the elastic form factor[6]. The model successfully explains the levelling off with k^2 and the region in k^2 where this levelling off occurs. This implies that we have included particles of approximately the correct mass in our exchange mechanism. It is rather surprising that this simple picture holds up to such high k^2.

[6] Thus only a scaling law for the elastic form factors is needed in the present theoretical calculation. We have assumed $G_{E_p} = G_{M_p}/\mu_p = G_{M_n}/\mu_n = -(4m^2/k^2)(G_{E_n}/\mu_n)$. Other proposed scaling laws do not significantly change the results in Figs 3–6 [11].

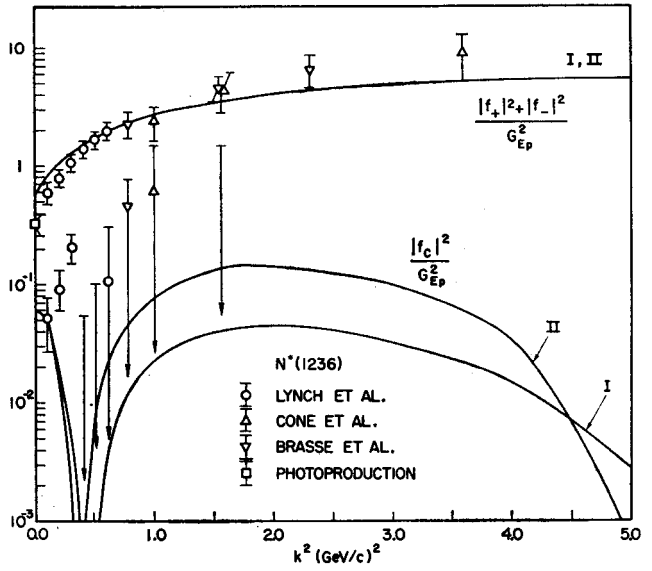

Fig. 10. $(|f_+|^2+|f_-|^2)/G_{Ep}^2$ and $|f_c|^2/G_{Ep}^2$ for the $3/2^+$, 3/2 (1236) resonance [11]. The predictions of models I and II (defined in the text) are indicated. The experimental points are from Ref. [24–26]. At the highest k^2 point from both Cone *et al.* and Brasse *et al.*, the cross-section has been assumed to be entirely transverse. The point at $k^2 = 0$ is determined from photoproduction data

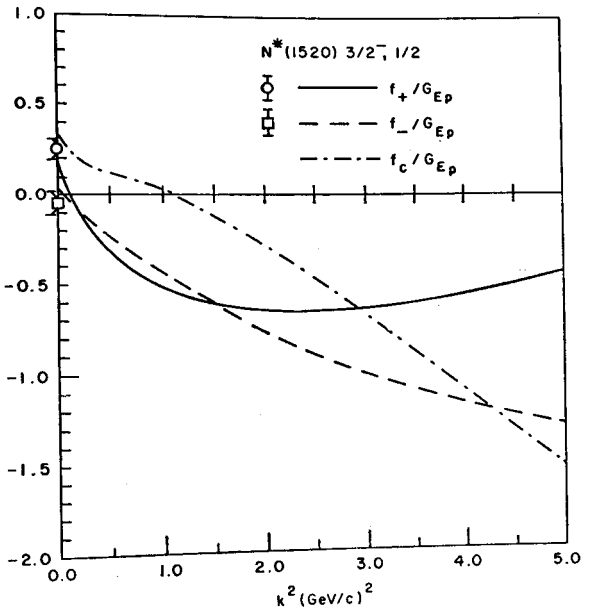

Fig. 11. Predictions of model II for f_+G_{Ep}, f_-/G_{Ep}, and f_c/G_{Ep} for excitation of the $3/2^-$, 1/2 (1520) resonance followed by decay into the $|\pi N\rangle$ final state [12]. To get the f's for decay into any final state, these amplitudes must be divided by $\cos \varepsilon_R = 0.71$. The points at $k^2 = 0$ come from photoproduction of pions

The similarity of the results of models I and II lends support to the theoretical analysis, but also indicates that the ratio $(d\sigma_{in}/d\sigma_{el})_{60}$ is not critically model dependent. This is evident since it is the sums of the squares of three amplitudes which is being measured (Eq. (1.18)). More model dependent are the individual coulomb and transverse contributions. A separation of these quantities for the $N^*(1236)$ has been carried out by Lynch at lower k^2 and the results are shown in Fig. 10 [11, 24–26]. Note the interesting predicted diffraction structure in $|f_c|^2$. The individual contributions f_c, f_+, and f_-, which can only be separated in a coincidence experiment, can be expected to show even more structure. Figure 11 shows the model II predictions for these quantities for the $3/2^-$, $1/2$ (1525) [12]. Note the diffraction feature in f_c at $k^2 \approx 1$ (GeV)^2.

3. A classical field model

A. Motivation
B. Hamiltonian and equations of motion
   i) Discussion of H
   ii) Ground-state field
   iii) Small oscillations of the field
C. Variational solution for the ground-state
D. Construction of the electromagnetic current
   i) Identification of the inelastic form factors
   ii) Construction of a conserved current
E. Ground-state properties
F. Some comparisons with experiment
G. Extensions of the model.

While the model discussed in the last lecture has the advantage of incorporating many general properties of the theory, it would be more satisfying to have a dynamical description of the origin of the resonances. The problem of a complete theory of strong-interaction dynamics is too hard, however, and we are forced to make models. In this lecture I will discuss a very simple-minded picture of the nucleon [27, 28, 14] which views it as a source sorrounded by a static, classical pion field. This field can then perform small oscillations about its equilibrium value, and the normal-mode oscillations of the pion field then provide a description of the excited states of the nucleon. The motivation for studying a classical-field model is twofold. First, the higher excited states of the nucleon correspond to many-meson states from a dispersion theory point of view, and present a formidable challange to dispersion theorists. We might hope to gain some insight with the classical limit of the theory, which corresponds to the presence of many (free) quanta. Second, it is intuitively appealing that there are shape oscillations of the meson field in the nucleon corresponding to the collective shape oscillations in nuclei, which show up strongly in inelastic electron scattering. What is, of course, sacrificed in this fixedsource model is Lorentz invariance, and therefore the calculated form factors can only give a qualitative picture if $k^2 \geq m^2$. The advantage of the model is that one can hope to have a consistent, self-contained dynamical description within this framework.

With these preliminaries, we proceed to write the hamiltonian [27]

$$H = \frac{1}{2}\int dx(\dot{\varphi}_\alpha\dot{\varphi}_\alpha+\nabla\varphi_\alpha\cdot\nabla\varphi_\alpha+\mu^2\varphi_\alpha\varphi_\alpha)+\frac{\lambda}{4}\int dx(\varphi_\alpha\varphi_\alpha)^2+$$

$$+\frac{1}{2}\int dx\beta(x)\varphi_\alpha\varphi_\alpha+\frac{G}{2m}\int dx(\boldsymbol{\sigma}\cdot\nabla\tau_\alpha\varphi_\alpha)s(x). \tag{3.1}$$

In this expression φ_α is a classical Klein-Gordon field, the subscripts $\alpha = 1, 2, 3$ denote isotopic spin, and repeated indices are summed. To the free Klein-Gordon hamiltonian we have added a fixed source of strength $Gs(x)/2m$, a potential $\beta(x)$ presumably coming from various particle exchange processes to scatter the field inside the source, and a term $\lambda(\varphi_\alpha\varphi_\alpha)^2/4 > 0$ which ensures that H has a ground state and which will contribute a potential barrier that makes it possible to have continuum resonances.

The energy of the system is clearly lowered if we set $\dot{\varphi}_\alpha = 0$, and we look for the static, ground-state field $\varphi^0_\alpha(x)$ by minimizing H

$$\frac{\delta H}{\delta\varphi_\alpha} = 0. \tag{3.2}$$

This results in a non-linear, inhomogeneous differential equation for φ^0_α

$$[\nabla^2-\mu^2-\lambda\varphi^0_\beta\varphi^0_\beta-\beta(x)]\varphi^0_\alpha(x) = -\frac{G}{2m}\tau_\alpha(\sigma\cdot\nabla)s(x). \tag{3.3}$$

If we now look for small oscillations of the field φ_α about the static value[7]

$$\varphi_\alpha(x,t) = \varphi^0_\alpha(x)+\eta_\alpha(x,t) \tag{3.4}$$

then η satisfies the equation

$$[\Box-\mu^2-\beta(x)-\lambda(\varphi^0_\beta\varphi^0_\beta)]\eta_\alpha = \lambda[\varphi^0_\alpha\varphi^0_\beta+\varphi^0_\beta\varphi^0_\alpha]\eta_\beta. \tag{3.5}$$

The ground-state field then provides an additional potential in which η_α moves. To make these equations tractable, a constant gradient source will be assumed

$$s(x) = \frac{3}{\pi a^3}(1-x/a)\theta(a-x) \tag{3.6}$$

and square-well potential

$$\beta(x) = -\beta\theta(a-x). \tag{3.7}$$

An exact solution to Eq. (3.3) is very difficult. We can, however, make use of the

[7] The expansion parameter here, η, is roughly $\eta^2 \approx \mu/\omega_{\mathrm{nl}}$ [27, 14].

fact that it was derived from a variational principle, Eq. (3.2), and look for a simple three-parameter variational solution [28, 14]. (Here $\hat{x} \equiv x/|x|$.)

$$\varphi_\alpha^0(x) = \tau_\alpha(\sigma \cdot \hat{x})\varphi^0(x)$$

$$\varphi^0(x) = c \qquad x<a$$

$$= c\left[\frac{e^{-\varrho(x-a)}}{x/a}(1-\varepsilon)+\frac{e^{-\mu(x-a)}}{x/a}\varepsilon\right] \qquad x>a. \tag{3.8}$$

In this expression it is assumed that $\tau_\alpha = \dot{\sigma}_\lambda = 0$ so that τ and σ are simply fixed vectors, the Pauli matrices, included only so that isospin and angular momentum can be treated consistently.[8] The function $\varphi^0(x)$ is taken as constant over the source and decays exponentially to the Yukawa tail.

The normal-mode equation for η_α now becomes simply

$$[\nabla^2+q^2-v(x)]\eta_\alpha = 0 \tag{3.9}$$

where $q^2 \equiv \omega^2-\mu^2$ and the potential $v(x)$ is sketched below. Equation (3.9) is just a Schrödinger equation, and the presence of the additional repulsive barrier for $x > a$

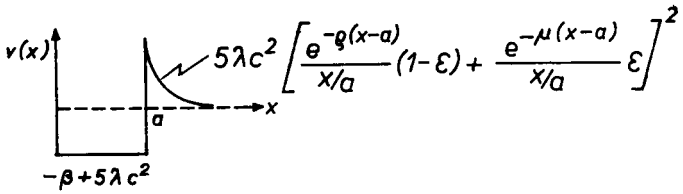

coming from the field φ_α^0 makes it possible to have continuum resonances as is the case for a real nucleon. To get a first orientation, we shall assume that the repulsive barrier is high enough so that it can be extended to infinity without appreciably changing the solutions for the low-lying states inside the potential well. If these solutions are denoted by $\eta_{nlm}(x)$ normalized to

$$\int dx \eta^\dagger_{n'l'm'}(x)\eta_{nlm}(x) = \delta_{nn'}\delta_{ll'}\delta_{mm'} \tag{3.10}$$

and the field is expanded as

$$\eta_\alpha(x, t) = \sum_{nlm}\frac{1}{\sqrt{2\omega_{nl}}}[\eta_{nlm}(x)e^{-i\omega_{nl}t}c^\alpha_{nlm}+\text{h.c.}] \tag{3.11}$$

then the hamiltonian in Eq. (3.1) takes the form [27]

$$H = E^0+\sum_{nlm\alpha}\omega_{nl}\tfrac{1}{2}[c^{\alpha\dagger}_{nlm}c^\alpha_{nlm}+c^\alpha_{nlm}c^{\alpha\dagger}_{nlm}]. \tag{3.12}$$

[8] The validity of this assumption can be checked by examining the coupled equations of motion for the spin and isospin. It turns out to be a reasonable approximation for the parameters we shall use for the higher nucleon resonances [28, 14].

The classical hamiltonian is now expressed in normal modes and at this point the normal-mode excitations of the field can be quantized in the canonical fashion.[9]

The resulting excitation spectrum for a choice of parameters

$$\mu a = 1$$

$$\beta a^2 - 5\lambda c^2 a^2 = 16 \tag{3.13}$$

is shown in Fig. 12. The spin 1/2 of the source must be coupled to the orbital excitations of the pseudoscalar meson field to yield the states $J = |l \pm 1/2|$, $\pi = (-1)^{l+1}$. These states will in general be split by some further spin-orbit interaction. Similarly, the isotopic spin 1/2 of the source must be coupled to the isospin 1 (Eq. (3.11)) of the meson field to

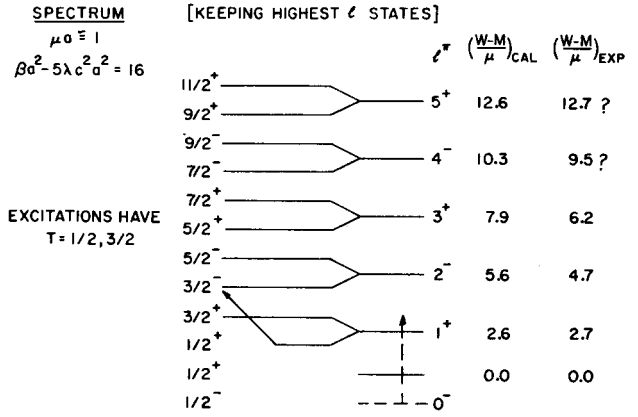

Fig. 12. Spectrum for the choice of parameters in the text. $\mu a = 1$, $\beta a^2 - 5\lambda c^2 a^2 = 16$. The energies are computed for a square-well potential with infinite walls and the total energy in the CM system, $W \equiv \equiv (q_{nl}^2 + \mu^2)^{1/2} + (q_{nl}^2 + m^2)^{1/2}$ is identified with the mass of the resonance [27, 28]

yield states with $T = 1/2$ and $3/2$. The lowest $1/2^-$ S-state in this potential is bound, and thus to get the experimental $1/2^+$ ground state, it must be assumed that this S-state, which samples the most interior regions of the nucleon, feels a weaker attractive potential than the other states. The $1/2^+$, $l = 1$ excited state will in general get pushed up by its interaction with the ground-state as indicated in Fig. 12. Thus the spectrum in Fig. 12 agrees roughly with that of the nucleon, although the actual forces evidently show a much stronger spin, orbital, and isospin dependence than this simple model suggests. The model does have the merit that every nucleon resonance which has been seen can be identified with one of the levels in this diagram.

The next problem is to construct the electromagnetic current operator for this system. Once the current and charge density have been obtained, the inelastic form factors

[9] The ground state of the nucleon is then $|0\rangle \xi_{m_s} \zeta_{m_t}$ where ξ_{m_s} and ζ_{m_t} are two-component spin and isospin Pauli spinors and $|0\rangle$ is the vacuum of the meson field excitations.

can be identified through the expressions familiar from nuclear physics [29]

$$|f_c|^2 = \frac{1}{2J_i+1}\sum_{J=0}^{\infty} |\langle J_f||\hat{M}_J^{\text{coul}}||J_i\rangle|^2$$

$$|f_+|^2+|f_-|^2 = \frac{1}{2J_i+1}\sum_{J=1}^{\infty} [|\langle J_f||\hat{T}_J^{\text{el}}||J_i\rangle|^2+|\langle J_f||\hat{T}_J^{\text{mag}}||J_i\rangle|^2] \tag{3.14}$$

where

$$\hat{M}_{JM}^{\text{coul}}(k^*) = \int j_J(k^*x)Y_{JM}(\Omega_x)\hat{\varrho}(x)dx$$

$$\hat{T}_{JM}^{\text{el}}(k^*) = \frac{1}{k^*}\int [\nabla \wedge j_J(k^*x)\mathcal{Y}_{JJ1}^M]\cdot \boldsymbol{j}(x)dx$$

$$\hat{T}_{JM}^{\text{mag}}(k^*) = \int [j_J(k^*x)\mathcal{Y}_{JJ1}^M]\cdot \boldsymbol{j}(x)dx. \tag{3.15}$$

To construct $j_\mu(x)$, we first replace $\nabla\varphi \to (\nabla - ieA)\varphi$ in H and obtain, from the coefficient of $-eA$ [28]

$$j_K(x) = -[\varphi \wedge \nabla_K\varphi]_3^{\text{sym}} + \frac{G}{2m}s(x)\sigma_K[\tau \wedge \varphi]_3^{\text{sym}} \qquad K = 1, 2, 3 \tag{3.16}$$

where the vector products refer to isospin. Now the aim is to construct a conserved current $\frac{\partial}{\partial x_\mu}j_\mu = 0$ so that the first-order S-matrix for the interaction of the target with an electromagnetic field

$$\hat{S}^{(1)} = ie\int d^4x\hat{j}_\mu(x)A_\mu^{\text{ext}}(x) \tag{3.17}$$

will be gauge invariant. In order to guarantee that the current be conserved, we define $-\nabla\cdot j \equiv \dot{\varrho}$ and use the equations of motion for φ_α to show

$$-\nabla\cdot\boldsymbol{j} \equiv \dot{\varrho} = \left[\varphi \wedge \frac{\partial^2\varphi}{\partial t^2}\right]_3^{\text{sym}} + \frac{G}{2m}s(x)\sigma_K[\nabla_K\varphi \wedge \tau]_3^{\text{sym}}. \tag{3.18}$$

Equations (3.16) and (3.18) are those obtained in the "standard theory" where the meson field is first coupled to a non-relativistic nucleon source $\hat{\psi}^+(x)\sigma\tau_\alpha\hat{\psi}(x)$ and then at the end of the calculation the replacement $\hat{\psi}^+(x)\sigma\tau_\alpha\hat{\psi}(x) \to s(x)\sigma\tau_\alpha$ is made. We have chosen to symmetrize the indicated expressions in Eq. (3.16) and (3.18) for simplicity and to avoid ambiguities in ordering. This symmetrization evidently makes no difference in the "standard theory". The first terms in Eqs (3.16), (3.18) are the familiar contributions of a Klein-Gordon field, and it is this part of the current which forms the most believable part of the model. The last two terms are "minimal" source contributions included for current conservation.

If the expressions (3.4) and (3.8) are substituted in Eqs (3.16), (3.18), then to first order in η_α [27]

$$j_K(x, t) = -[\varphi^0 \wedge \nabla_K \varphi^0]_3^{\text{sym}} - [\varphi^0 \wedge \nabla_K \eta]_3 - [\eta \wedge \nabla_K \varphi^0]_3 + \\ + \frac{G}{2m} s(x)\sigma_K[\tau \wedge \eta]_3 \qquad K = 1, 2, 3 \tag{3.19}$$

$$-\nabla \cdot j \equiv \dot{\varrho} = \left[\varphi^0 \wedge \frac{\partial^2 \eta}{\partial t^2}\right]_3 + \frac{G}{2m} s(x)\sigma_K[\nabla_K \eta \wedge \tau]_3. \tag{3.20}$$

The terms linear in η_α are linear in the creation and destruction operators for the normal--mode excitations, Eq. (3.11), and therefore can create any of the one-quantum excitations from the ground-state.

The expression (3.20) can be integrated once with respect to time to give

$$\varrho(x, t) = \frac{1}{2}(1+\tau_3)s(x) + \left[\varphi^0 \wedge \frac{\partial \eta}{\partial t}\right]_3 + \frac{G}{2m} s(x)\sigma_K[\nabla_K \bar{\eta} \wedge \tau]_3 + \\ + \left[\eta \wedge \frac{\partial \eta}{\partial t}\right]_3 \tag{3.21}$$

where the first term is an integration constant and the last term bilinear in η has been included since it is a known part of the Klein-Gordon charge density. $\bar{\eta}_\alpha$ is defined by

$$\bar{\eta}_\alpha \equiv i \sum_{nlm} \frac{1}{\sqrt{2\omega_{nl}^3}} [\eta_{nlm}(x) e^{-i\omega_{nl}t} c_{nlm}^\alpha - \text{h.c.}] \tag{3.22}$$

and satisfies $\dfrac{\partial \bar{\eta}_\alpha}{\partial t} = \eta_\alpha$. We may now make the following observations on the results (3.19)–(3.22):

i) In a "fully-linearized theory", where the right-hand side of Eq. (3.5) is neglected so that the potentials appearing on the left-hand side of Eqs (3.3) and (3.5) are identical, the relation

$$\nabla \cdot j + \dot{\varrho} = 0 \tag{3.23}$$

can be verified from the equations of motion (3.3), (3.5) and Eq. (3.8). Furthermore, the total charge obtained from Eq. (3.21) is

$$Q = \int \varrho(x, t) dx = \frac{1}{2}(1+\tau_3) + \int \left[\eta \wedge \frac{\partial \eta}{\partial t}\right]_3 dx = \frac{1}{2} + T_3 \tag{3.24}$$

which again follows directly from a partial integration and the use of the equation of motion (3.3), (3.5) and Eq. (3.8). Since this is the desired definition of Q, and $[\hat{Q}, \hat{H}] = 0$ when the normal-mode excitations are quantized, our definitions of j and ϱ are satisfactory from this point of view.

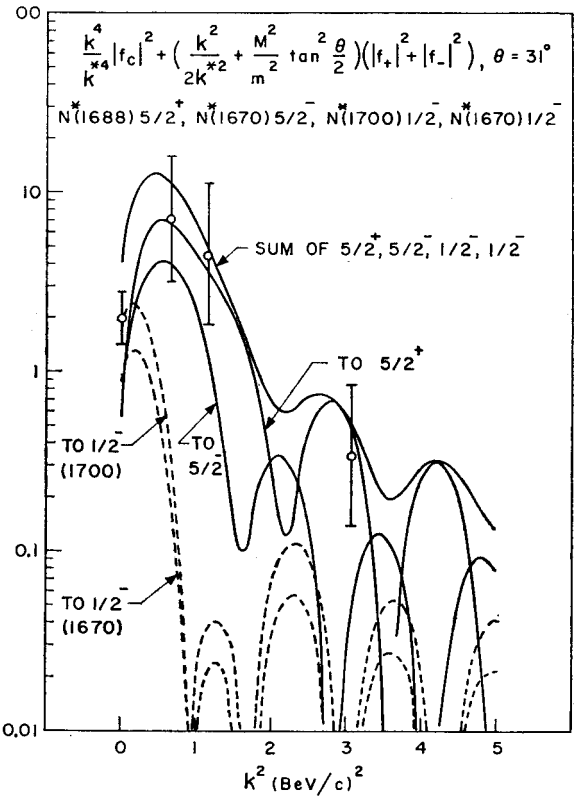

Fig. 13. Reduced inelastic electron scattering transition probability $\left[\frac{k^4}{k^{*4}}|f_c|^2+\left(\frac{k^2}{2k^{*2}}+\frac{M^2}{m^2}\tan^2\frac{\theta}{2}\right)(|f_+|^2+|f_-|^2)\right]_{31°}/\mu a(ca)^2$ for the $5/2^+$, 1/2 (1688) resonance region [28, 14]. The data is from the CEA group [25]. The background resonances which are also thought to resonate in this region have also been included. Note the ordinate must still be multiplied by $\mu a(ca)^2 = 0.010$ to get the experimental form factors

ii) In the present theory where the right side of Eq. (3.5) is retained and computed from Eq. (3.8), it is necessary to add terms

$$\delta\hat{\varrho} = 2\lambda(\varphi^0)^3(\boldsymbol{\sigma}\cdot\hat{\boldsymbol{x}})[\boldsymbol{\tau}\wedge\boldsymbol{\eta}]_3 \tag{3.25a}$$

$$\delta\varrho = 2\lambda(\varphi^0)^3(\boldsymbol{\sigma}\cdot\hat{\boldsymbol{x}})[\boldsymbol{\tau}\wedge\bar{\boldsymbol{\eta}}]_3 \tag{3.25b}$$

to have Eqs (3.23) and (3.24) follow identically from the model equations of motion. With the parameters we shall use, these terms do not play an important role in the theory [28, 14]. They have the disadvantage, however, that they depend on the parameter λ which is only very poorly determined in our calculations. In general, we have preferred to use expressions (3.19) and (3.21), regarding these as approximations to the current and charge density in the "standard theory".

The current (3.19) and charge density (3.21) have ground-state expectation values, leading to the following expressions for the charge form factors

$$G_E^s(k^*) = G_E^v(k^*) = \int e^{ik^*x} s(x)dx \tag{3.26}$$

and for the meson contribution to the anomalous magnetic moment form factors

$$\lambda^v(k^*) = \frac{4m}{3}\int\left[\frac{3j_1(k^*x)}{k^*x}\right][\varphi^0(x)]^2 dx \tag{3.27}$$

$$\lambda^s(k^*) = 0 \tag{3.28}$$

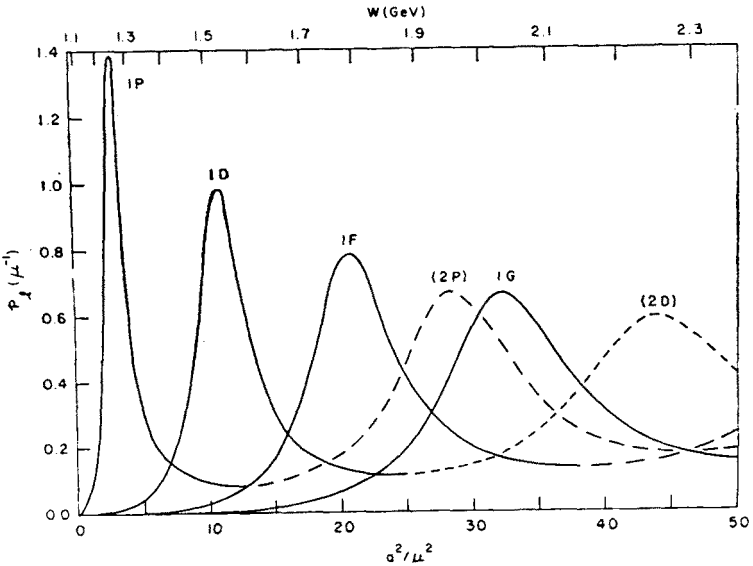

Fig. 14. Resonance spectrum for the square-well potential with a square-well barrier described in the text. The ordinate is the integrated square of the wave function inside the barrier

$$P_l = \int_0^{r_1} dx |qR_{q,l}(x)|^2 |Y_{lm}|^2 \text{ in units of } 1/\mu$$

In addition, the pion-nucleon coupling constant can be related to another ground-state property, the Yukawa tail of the pion field, and it follows from Eqs (3.8) that

$$f_{\pi N}^2 = \frac{G_{\pi N}^2}{4\pi}\left(\frac{\mu}{2m}\right)^2 = 4\pi\varepsilon^2(ca)^2 e^{2\mu a} \tag{3.29}$$

In Refs [28, 14] the implications of this model are compared with experiment. The parameters used there are

$$\mu a = 1$$

$$\beta a^2 - 5\lambda c^2 a^2 = 16$$

$$5\lambda c^2 a^2 \cong 40 \tag{3.30}$$

chosen to fit the spectrum (Fig. 12). The last relation comes from demanding that the repulsive barrier be high enough to make the states we are interested in show up as resonances.[10] Using these numbers, ϱ, ε, and

$$\alpha = \frac{G}{2(ma)\,(ca)} \cong 10 \tag{3.31}$$

are obtained by minimizing E_0 using the variational form (3.8) and a value

$$\mu a(ca)^2 = 0.010 \tag{3.32}$$

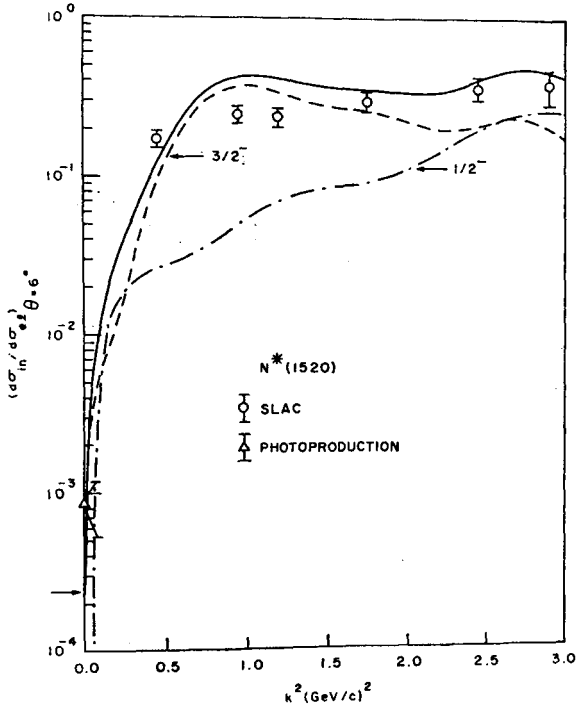

Fig. 15. $d\sigma_{in}/d\sigma_{el}$ at 6° for the 1520 MeV region in the classical-field model [14]. (Both theory and experiment are divided by the experimental $d\sigma_{el}$ — see text). The experimental points are from Ref. [4]. The contributions of the 3/2⁻, 1/2 (1520) and 1/2⁻, 1/2 (1535) states calculated in the model are shown separately

is obtained by fitting the height of the inelastic form factors. One example of the fit to the inelastic form factors obtained with these parameters is shown in Fig. 13. This is for the 1688 MeV resonance and the experimental points are from the original work by the CEA group [25]. Here all the known individual contributions in this resonance region are computed using this model. Note that the 5/2⁺, 1/2(1688) again dominates the spectrum. Some further consequences of this version of the model are:

i) The same normalization (3.32) fits the strength of the 1525 and 1950 MeV resonances,

[10] λ cannot be too large, for then the zero-point oscillations of the field become important [30, 27].

and the model gives qualitatively the correct overall shape for these form factors. These curves are given in Ref. [28]. One problem is that the presence of the sharp square well and repulsive potentials gives rise to diffraction minima which are not seen experimentally.

ii) The charge and magnetic moment radii computed from Eq. (3.26), (3.27) are

$$(\langle r^2\rangle_E^s)^{1/2} = (\langle r^2\rangle_E^v)^{1/2} = 0.89 \text{ fm}$$

$$(\langle r^2\rangle_M^v)^{1/2} = 1.04 \text{ fm}.$$

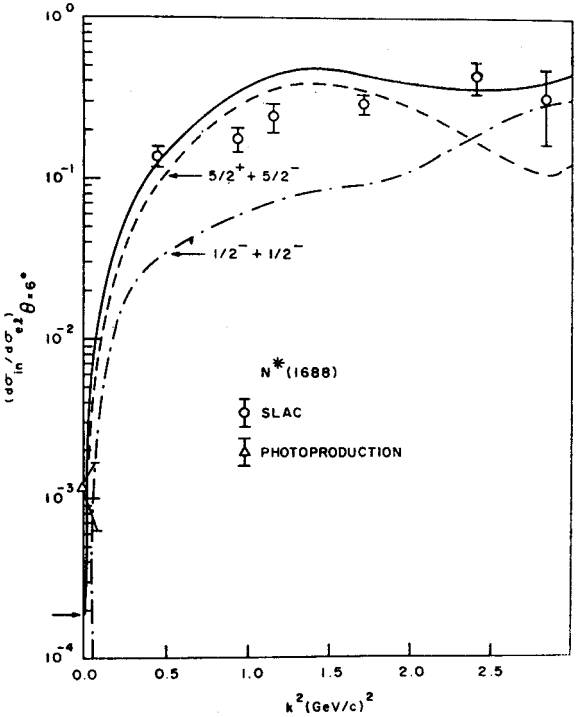

Fig. 16. Same as Fig. 15 for the 1688 MeV region. The contributions of the two spin 5/2, and two spin 1/2 states are shown separately

These are to be compared with the experimental values of 0.8 fm. Thus the size of the nucleon is approximately correct in the model.

iii) Using Eq. (3.32), which was determined from the inelastic form factors, Eq. (3.27) gives $\lambda^v(0) = +0.6$ while the experimental value of this quantity is $\lambda^v(0) = +1.85$. This is at least in the right ballpark.

iv) Equation (3.29) and the parameters above give $f_{\pi N}^2 = 0.01$ while the experiment value is $f_{\pi N}^2 = 0.08$. This quantity is only very poorly determined in the model since it depends on how the field itself penetrates the repulsive barrier out to the tail. Again, the number is at least in the right ballpark.

Pritchett [14, 31] has recently extended this model in several ways:

i) In an attempt to eliminate the spurious diffraction minima, the excited state wave functions are computed as actual continuum solutions in a potential of the form

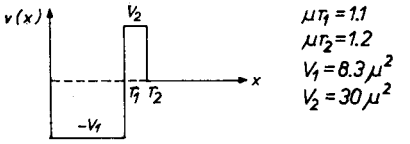

whose parameters are chosen to give the spectrum shown in Fig. 14. In this picture the widths of the resonances can also be calculated. The resulting spectrum is not unreasonable. Again, the $1/2^-$, $l = 0$ bound state must be artificially pushed to high energy.

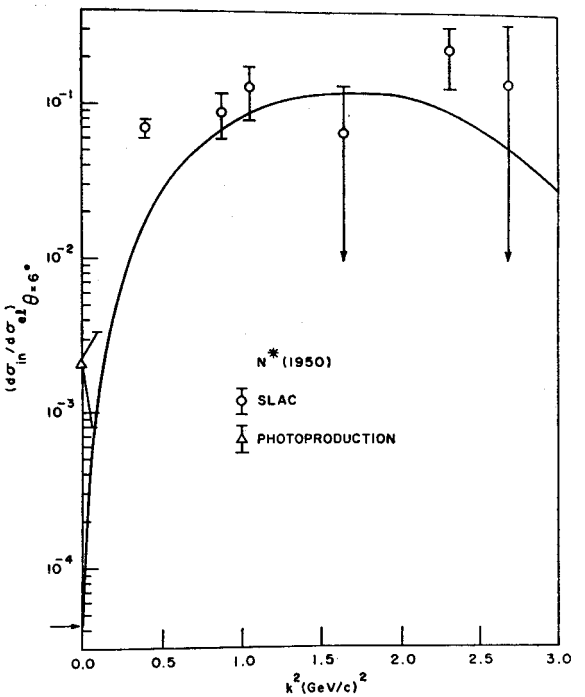

Fig. 17. Same as Fig. 14 for the 1950 MeV region [7/2+, 3/2 (1950)]

ii) Equation (3.26) is inverted using the experimental charge form factor to find a more realistic source function $s(x)$.

iii) Equation (3.27) is inverted to find a (smoother) form for the ground-state field $\varphi_0(x)$.

iv) $\beta(x)$ is determined from the relation $v(x) = \beta(x) + 5\lambda[\varphi^0(x)]^2$ and E^0 is still minimized yielding relations on the coupling constants in the model. The values $\lambda = 20$ and $G = 12$ are consistent with these restrictions and suppress the S-wave contributions as indicated by photoabsorption. (Pritchett includes the terms (3.25) in his charge density.)

All the parameters in the theory are now determined and Figs 15–18 show a comparison between the theoretical values of $d\sigma_{in}$ at 6° and the SLAC data (both theory and experiment

have been divided by the experimental value of $d\sigma_{el}$ as explained previously) for the 1525, 1688, 1950, and 1236 resonances. The general shape and magnitudes are fairly good (with a few noticeable discrepancies) except for the 1236 where the theoretical curve (dotted line) is too low. The "highest-l" resonances again dominate the observed resonance regions over most of the range of k^2.

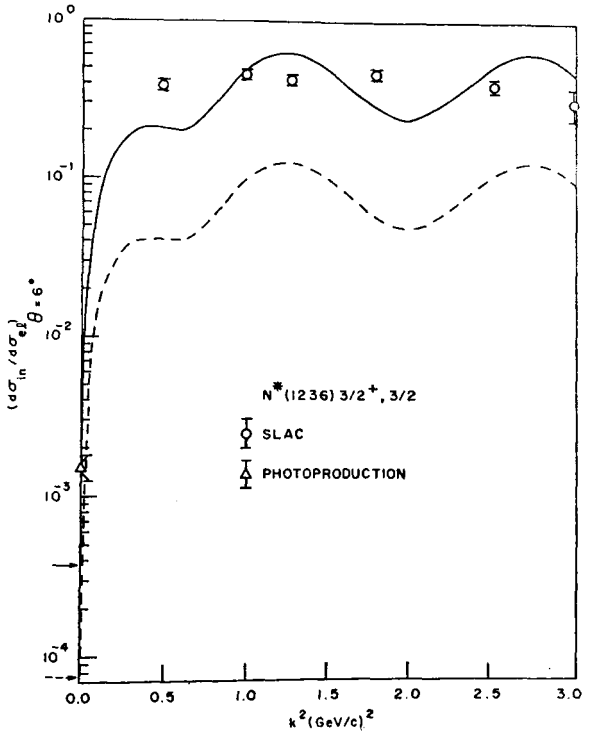

Fig. 18. Same as Fig. 14 for the $3/2^+$, 3/2 (1236) level. The broken line is the result of Pritchett's calculation. The solid line is theory × 5

The model as developed so far is a very naive one. Even within the framework of the model there are many improvements that could be made such as finding a mechanism for the generation of the potential $\beta(x)$, including the vacuum fluctuations of the meson field correctly [27], and taking some steps towards making the model Lorentz invariant. Despite its shortcomings, the model does provide a dynamical framework in which to investigate the electromagnetic properties of the nucleon, and the interrelations between these quantities, on a consistent basis.

REFERENCES

[1] S. D. Drell, J. D. Walecka, *Ann. Phys.* (USA), **28**, 18 (1964).

[2] J. D. Bjorken (unpublished); R. Von Gehlen, *Phys. Rev.*, **118**, 1455 (1960); M. Gourdin, *Nuovo Cimento*, **21**, 1094 (1961).

[3] E. Bloom, D. Coward, H. DeStaebler, J. Drees, J. Litt, G. Miller, L. Mo, R. E. Taylor, M. Breidenbach, J. I. Freidman, H. W. Kendall, S. Loken, SLAC Group A, reported by

W. K. Panofsky, in *International Conference on High-Energy Physics*, Vienna 1968 (CERN, Geneva 1968, p. 23).
[4] M. Breidenbach, *Ph. D. Thesis*, Massachusetts Institute of Technology, 1971 (unpublished).
[5] L. Durand, P. deCelles, R. Marr, *Phys. Rev.*, **126**, 1882 (1962).
[6] J. D. Bjorken, J. D. Walecka, *Ann. Phys.* (USA), **38**, 35 (1966).
[7] M. Jacob, G. C. Wick, *Ann. Phys.* (USA), **7**, 404 (1959).
[8] A. R. Edmonds, *Angular Momentum in Quantum Mechanics*, Princeton University Press, Princeton, New Jersey (1959).
[9] S. Fubini, Y. Nambu, V. Wataghin, *Phys. Rev.*, **111**, 329 (1958).
[10] J. D. Walecka, P. A. Zucker, *Phys. Rev.*, **167**, 1479 (1968).
[11] P. L. Pritchett, J. D. Walecka, P. A. Zucker, *Phys. Rev.*, **184**, 1825 (1969).
[12] P. L. Pritchett, P. A. Zucker, *Phys. Rev.*, *D***1**, 175 (1970).
[13] P. A. Zucker, *Ph. D. Thesis*, Stanford University, 1970 (unpublished).
[14] P. L. Pritchett, *Ph. D. Thesis*, Stanford University, 1970 (unpublished).
[15] K. M. Watson, *Phys. Rev.*, **88**, 1163 (1952).
[16] R. Omnès, *Nuovo Cimento*, **8**, 316 (1958).
[17] P. Dennery, *Phys. Rev.*, **124**, 2000 (1961).
[18] N. Zagury, *Phys. Rev.*, **145**, 1112 (1966).
[19] F. Gutbrod, D. Simon, DESY *Report* No 67/1, 1967.
[20] R. C. Vik, *Phys. Rev.*, **163**, 1535 (1967).
[21] S. L. Adler, *Ann. Phys.* (USA), **50**, 189 (1968).
[22] Y. Yamaguchi, *Progr. Theor. Phys. Suppl.*, **7**, 1 (1959).
[23] G. F. Chew, M. L. Goldberger, F. E. Low, Y. Nambu, *Phys. Rev.*, **106**, 1337 (1957).
[24] H. L. Lynch, J. V. Allaby, D. M. Ritson, *Phys. Rev.*, **164**, 1635 (1967).
[25] A. A. Cone, K. W. Chen, J. R. Dunning, Jr., G. Hartwig, Norman Ramsey, J. K. Walker, Richard Wilson, *Phys. Rev.*, **156**, 1490 (1967); **163**, 1854 (E) (1967).
[26] F. W. Brasse, J. Engler, E. Ganssauge, M. Schweizer, *Nuovo Cimento*, **55A**, 679 (1968).
[27] J. D. Walecka, *Phys. Rev.*, **162**, 1462 (1967).
[28] P. L. Pritchett, J. D. Walecka, *Phys. Rev.*, **168**, 1638 (1968).
[29] T. deForest, J. D. Walecka, *Advances in Phys.*, **15**, 1 (1966).
[30] D. Yennie, *Phys. Rev.*, **88**, 527 (1952).
[31] P. L. Pritchett, DESY *preprint* (1971).